Aerotecnica Missili & Spazio, *The Journal of Aerospace Science, Technology and Systems*

Comparisons between 1D (Beam) and 2D (Plate/Shell) Finite Elements to Analyze Thin Walled Structures

E. Carrera[a], M. Cinefra[a], M. Petrolo[b], E. Zappino[a]

[a] Politecnico di Torino
Department of Mechanical and Aerospace Engineering

[b]RMIT University - Royal Melbourne Institute of Technology
School of Aerospace, Mechanical and Manufacturing Engineering

Abstract

This paper compares 1D and 2D assumptions for the analysis of isotropic thin-walled structures. Refined 1D (beam) and 2D (shell) models were exploited. These models are based on a variable kinematic approach which means that the displacement field assumed can be refined to any extent since the orders of the polynomial expansions are taken as free parameters. The Finite Element (FE) approach was used to provide numerical results. FEM is, in fact, the most popular technique used in the analysis of structures in engineering. The Carrera Unified Formulation (CUF) was adopted in order to write finite element matrices of 1D and 2D models in a concise form based on the so-called fundamental nuclei. In this work, 1D models are used to assess well established benchmarks which are often used to solve shell problems, such as the pinched shell problem. 1D and 2D models were compared in terms of accuracy and computational costs. Furthermore, locking phenomena are discussed. It is concluded that some of the well-known shell problems, including those that are usually used as 'benchmarks' in FE shell developments, can be dealt with 1D refined models. The use of 1D refined models results in minor numerical locking, much lower computational efforts and comparable accuracy with shell models.

1. Introduction

Theories of structures (TOS) can be built according to various methods. If only displacement variables are considered, the fundamental problem of TOS will consist of the evaluation of the minimum number of unknown variables (UVs) needed to solve a given problem according to a fixed accuracy. In the development of the so-called axiomatic approach to TOS, UVs are introduced by postulating an expansion for the three unknown displacements. Such an expansion can be formulated in many different ways. The generic displacement component u in an orthogonal reference system (x, y, z) can be expanded in terms of one-dimensional (1D) or two-dimensional (2D) UVs, respectively,

$$\begin{aligned} 1D: u = u_i^{1D}(y)\ F_i^{1D}(x,z), \qquad i = 1,..,M_{1D} \\ 2D: u = u_i^{2D}(x,y)\ F_i^{2D}(z), \qquad i = 1,...,M_{2D} \end{aligned} \tag{1}$$

where $u_i^{1D}(y)$ and $u_i^{2D}(x,y)$ are UVs , F_i^{1D} and F_i^{2D} are the base functions used for the 1D and 2D expansions. It is assumed that in the 1D case the expansion is made in terms of the two coordinates x, z (over a given section for a given y-value) while the expansion is made in terms of z (over the thickness at a given point of coordinates x, y) for 2D models. The base functions can be represented by any kind of polynomials, such as powers of z (or x, z in the 1D cases), harmonics, Lagrange, Legendre, etc. The Principle of Virtual Displacements (PVD) can be used to derive governing equations (in both weak and strong forms) consistent with the assumptions made in Eq. 1.

This work deals with the analysis of shell structures by means of 1D and 2D structural models. 1D theories are usually referred to as 'beam' models. The best known examples are the Euler-Bernoulli [1] and Timoshenko [2, 3] models. These models are hereafter referred to as EBBT and TBT, respectively. EBBT and TBT provide reliable results when the bending of compact structures made of isotropic materials is considered. Higher-order beam models are needed to account for the non-classical effects due to, for instance, thin walls or point loads. An excellent review on higher-order models can be found in [4]. Many methods have been proposed to overcome the limitations of classical theories and to allow the application of 1D models to any geometries or boundary conditions as discussed in [5]. Most recent developments in 1D models have been obtained by means of the following approaches: the introduction of shear correction factors [6]; the use of warping functions based on the de Saint-Venant solution [7–10]; the variational asymptotic solution (VABS) [11, 12]; Generalized beam theories (GBT) [13–17].

It is known that when a finite element method is used to discretize a physical model, the phenomenon of numeri-

cal *locking* may arise from hidden constrains which are not well represented in the finite element approximation. Many approaches have been proposed to overcome the locking phenomenon, such as the use of the standard displacement formulation with higher-order elements [18, 19], the use of reduced-selective integration techniques [20, 21] or the use of modified variational forms [22].
In this work, typical shell problems were assessed by means of 1D structural problems, results from 1D theories were then compared to those from shell models. 1D and shell models were derived from the Carrera Unified Formulation (CUF) [23]. In the CUF framework, higher-order structural models are hierarchically obtained since the order of the model is considered as an input of the analysis. A cylindrical shell finite element based on CUF [24] is adopted in this paper. As in [25] and in [26], the Mixed Interpolation of Tensorial Components (MITC) method has been extended to shell elements with nine nodes in order to eradicate membrane and shear locking. The performances of these elements were tested in [27] by solving discriminating problems from the literature which involved very thin shells.
CUF higher-order 1D models have recently been developed by Carrera and coworkers [28–30]. Static [30–32], free-vibration [33–35] and buckling [36] analyses showed the enhanced capabilities of CUF 1D models which are able to detect shell- and solid-like solutions for different structural models including thin-walled structures under point loads and shell-like natural modes. As a result of a further extension of the present formulation [37, 38], open cross-sections, boundary conditions enforced on lateral edges and layer-wise approaches were also dealt with. Another recent extension of CUF is the so-called mixed axiomatic-asymptotic technique [39–42] which enables the evaluation of the contribution of each term of the expansion on the prediction of the mechanical response of a structure.
This paper represents an effort to provide a comprehensive comparison campaign between 1D and shell models in order to show how the use of higher-order 1D theories can be effective in detecting shell-like solutions.
This paper comprises a brief theoretical introduction of CUF for beams and shells and related finite element formulations. Numerical results related to thin walled structures are then presented with particular attention given to pinched shells and the Scordelis-Lo roof problem.

2. Carrera Unified Formulation (CUF)

In the CUF framework, the displacement field of a structural model is the expansion of generic functions F_τ,

$$\mathbf{u} = F_\tau \mathbf{u}_\tau, \qquad \tau = 1, 2, ..., M \tag{2}$$

where $\mathbf{u}$ is the displacement vector, $\mathbf{u}_\tau$ is the generalized displacements unknown array and M stands for the number of terms of the expansion. According to the Einstein notation, the repeated subscript, τ, indicates summation. The expression given by Eq. 2 is valid for both 1D and 2D models since these models are obtained by acting on the expansion functions F_τ. In fact,

$$\begin{gathered} 1D: \mathbf{u}(x,y,z) = F_\tau(x,z)\mathbf{u}_\tau(y), \tau = 1, 2, ..., M_{1D} \\ 2D - Shell: \mathbf{u}(\alpha,\beta,z) = F_\tau(z)\mathbf{u}_\tau(\alpha,\beta), \tau = 1, 2, ..., M_{2D} \end{gathered} \tag{3}$$

where α and β are the in-plane curvilinear coordinates. In the case of 1D models, the expansions of the displacement field relate to the cross-section coordinates (x, z) while the unknowns of the problem are given in a certain location above the cross-section. In the case of 2D models, the expansions are related to the thickness coordinate (z) and the unknowns are given in a certain point along z. The choice of F_τ determines which class of CUF models to adopt.

2.1. CUF 1D models, TE and LE classes; 1D variable kinematic assumptions

Two classes of 1D CUF models were adopted in this paper, the Taylor Expansion class (TE) and the Lagrange Expansion class (LE). This means that two different types of F_τ expansions were exploited with no need to make a formal modification of the unified formulation.
TE is based on Taylor-like polynomial expansions, $x^i\, z^j$, of the displacement field above the cross-section of the structure (i and j are positive integers). The order (N) of the expansion is arbitrary and is set as an input of the analysis. For example, the second-order model, $N = 2$, is based on the the following expansion:

$$\begin{aligned} u_x &= u_{x_1} + x\, u_{x_2} + z\, u_{x_3} + x^2\, u_{x_4} + xz\, u_{x_5} + z^2\, u_{x_6} \\ u_y &= u_{y_1} + x\, u_{y_2} + z\, u_{y_3} + x^2\, u_{y_4} + xz\, u_{y_5} + z^2\, u_{y_6} \\ u_z &= u_{z_1} + x\, u_{z_2} + z\, u_{z_3} + x^2\, u_{z_4} + xz\, u_{z_5} + z^2\, u_{z_6} \end{aligned} \tag{4}$$

The 1D model described by Eq. 4 has 18 generalized displacement variables; three constant, six linear, and nine parabolic terms. Classical beam theories, Euler-Bernoulli (EBBT) and Timoshenko (TBT), can be obtained as particular cases of the $N = 1$ model, as shown in [30]. A convergence study is usually needed to choose N for a given structural problem.
LE exploits Lagrange polynomials to build 1D refined models. In this paper, two types of cross-section elements were adopted: nine-point elements and sixteen-point elements hereafter referred to as L9 and L16, respectively. These elements are shown in Fig. 1. The isoparametric formulation was exploited to deal with arbitrary shaped geometries. The L9 interpolation polynomials are given in [43]

$$\begin{gathered} F_\tau = \tfrac{1}{4}(r^2 + r\, r_\tau)(s^2 + s\, s_\tau) \qquad \tau = 1, 3, 5, 7 \\ F_\tau = \tfrac{1}{2}s_\tau^2(s^2 - s\, s_\tau)(1 - r^2) + \tfrac{1}{2}r_\tau^2(r^2 - r\, r_\tau)(1 - s^2) \\ \tau = 2, 4, 6, 8 \\ F_\tau = (1 - r^2)(1 - s^2) \qquad \tau = 9 \end{gathered} \tag{5}$$

where r and s range from -1 to $+1$ and where r_τ and s_τ are the natural coordinates of the interpolation points above

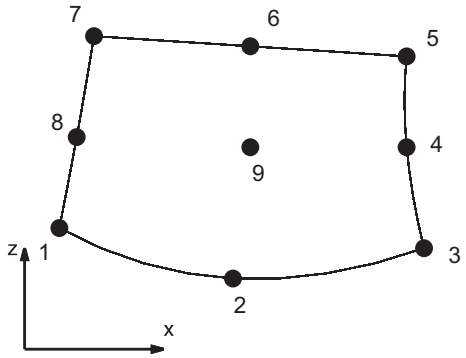

(a) Nine-point element, L9

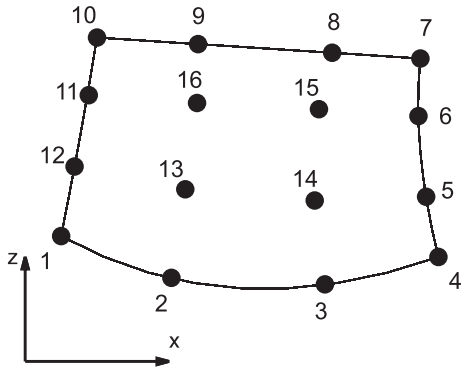

(b) Sixteen-point element, L16

Figure 1. Cross-Section elements of the LE class

the cross-section. The displacement field given by an L9 element is

$$\begin{aligned} u_x &= F_1\, u_{x_1} + F_2\, u_{x_2} + F_3\, u_{x_3} + ... + F_8\, u_{x_8} + F_9\, u_{x_9} \\ u_y &= F_1\, u_{y_1} + F_2\, u_{y_2} + F_3\, u_{y_3} + ... + F_8\, u_{y_8} + F_9\, u_{y_9} \\ u_z &= F_1\, u_{z_1} + F_2\, u_{z_2} + F_3\, u_{z_3} + ... + F_8\, u_{z_8} + F_9\, u_{z_9} \end{aligned} \tag{6}$$

where $u_{x_1}, ..., u_{z_9}$ are the displacement variables of the problem and they represent the pure displacement components of each of the nine points of the L9 element. This means that LE models provide elements having only pure displacement variables. L16 models are obtained in the same manner, the explicit expression of these polynomials are not reported here, they can be found in [38,43]. It is important to underline that multiple L-elements can be assembled in order to locally refine the 1D model.

2.2. CUF shell models: 2D variable kinematic assumptions

The application of a two-dimensional method for shells permits one to express the unknown variables as a set of thickness functions depending only on the thickness coordinate z and the corresponding variables depending on the in-plane curvilinear coordinates α and β. A Taylor expansion was here employed as the thickness function $F(z)$,

$$\begin{gathered} \boldsymbol{u} = F_0\, \boldsymbol{u}_0 + F_1\, \boldsymbol{u}_1 + \ldots + F_N\, \boldsymbol{u}_N = F_\tau\, \boldsymbol{u}_\tau \\ with \;\; \tau = 0, 1, \ldots, N \end{gathered} \tag{7}$$

$$F_0 = z^0 = 1, \;\; F_1 = z^1 = z, \;\; \ldots, \;\; F_N = z^N \tag{8}$$

For example, the second-order model is based on the the following expansion:

$$\begin{aligned} u_x &= u_{x_1} + z\, u_{x_2} + z^2\, u_{x_3} \\ u_y &= u_{y_1} + z\, u_{y_2} + z^2\, u_{y_3} \\ u_z &= u_{z_1} + z\, u_{z_2} + z^2\, u_{z_3} \end{aligned} \tag{9}$$

It is possible to obtain the first order shear deformation theory (FSDT) model [44] from a first-order expansion theory by considering a constant transverse displacement through the thickness. An appropriate application of penalty techniques to the shear correction factor leads to the classical lamination theory (CLT) model [45].
The strain-displacement relations are given by the linear part of the *3D Green Lagrange strain tensor*, see Appendix A.

3. FE Formulation and the Fundamental Nucleus

The Finite Element (FE) approach was adopted to deal with arbitrary geometries and boundary conditions. FEs were developed via a classical finite element methodology based on the Principle of Virtual Displacements. The shape functions, N_i, and the nodal displacement vector, $\mathbf{q}_{\tau i}$, are used and the displacement vectors become

$$\begin{aligned} 1D: \quad & \mathbf{u}(x,y,z) = N_i(y) F_\tau(x,z) \mathbf{q}_{\tau i}, \\ & i = 1, 2, ..., K_{1D} \\ 2D - Shell: \quad & \mathbf{u}(\alpha,\beta,z) = N_i(\alpha,\beta) F_\tau(z) \mathbf{q}_{\tau i}, \\ & i = 1, 2, ..., K_{2D} \end{aligned} \tag{10}$$

with

$$\mathbf{q}_{\tau i} = \left\{ \begin{array}{ccc} q_{u_{x_{\tau i}}} & q_{u_{y_{\tau i}}} & q_{u_{z_{\tau i}}} \end{array} \right\}^T \tag{11}$$

K_{1D} is the number of the nodes on the 1D element, elements with 4 nodes (B4) were used in this paper . K_{2D} is the number of the nodes on the shell element, elements with 9 nodes (Q9) were used in this paper. For the sake of brevity, the explicit forms of the shape functions, N_i, are not reported here, they can be found in [46].
The stiffness matrix is obtained via the Principle of Virtual Displacements,

$$\delta L_{int} = \delta L_{ext} \tag{12}$$

L_{int} stands for the strain energy and L_{ext} is the work of the external loadings. δ stands for the virtual variation.

3.1. 1D finite elements

The virtual variation of the strain energy is given by

$$\delta L_{int} = \int_V (\delta \boldsymbol{\epsilon}^T \boldsymbol{\sigma}) dV = \\ = \int_V \delta \mathbf{q}_{\tau i}^T \Big[\boldsymbol{D}^T \Big(N_i(y) F_\tau(x,z) \boldsymbol{I} \Big) \Big] \boldsymbol{C} \Big[\boldsymbol{D} \Big(N_j(y) F_s(x,z) \boldsymbol{I} \Big) \Big] \mathbf{q}_{sj} dV \tag{13}$$

By exploiting geometrical relations and the unified formulation, it is possible to rewrite the virtual variation of L_{int} as

$$\begin{aligned} \delta L_{int} &= \delta \mathbf{q}_{\tau i}^T \Bigg\{ \int_V \Big[\Big(\boldsymbol{D}_\Omega + \boldsymbol{D}_y \Big)^T \Big(F_\tau(x,z) N_i(y) \boldsymbol{I} \Big) \Big] \boldsymbol{C} \\ &\quad \Big[\Big(\boldsymbol{D}_\Omega + \boldsymbol{D}_y \Big) \Big(N_j(y) F_s(x,z) \boldsymbol{I} \Big) \Big] dV \Bigg\} \mathbf{q}_{sj} = \\ &= \delta \mathbf{q}_{\tau i}^T \Bigg\{ \int_l \Big(N_i(y) \Big(\int_\Omega \Big[\boldsymbol{D}_\Omega^T \Big(F_\tau(x,z) \boldsymbol{I} \Big) \Big] \boldsymbol{C} \\ &\quad \Big[\boldsymbol{D}_\Omega \Big(F_s(x,z) \boldsymbol{I} \Big) \Big] d\Omega \Big) N_j(y) \Big) dy + \\ &\quad + \int_l \Big(N_i(y) \Big(\int_\Omega \Big[\boldsymbol{D}_\Omega^T \Big(F_\tau(x,z) \boldsymbol{I} \Big) \Big] \boldsymbol{C} \\ &\quad F_s(x,z) d\Omega \Big) \boldsymbol{D}_y \Big(N_j(y) \boldsymbol{I} \Big) \Big) dy + \\ &\quad + \int_l \Big(\boldsymbol{D}_y^T \Big(N_i(y) \boldsymbol{I} \Big) \Big(\int_\Omega F_\tau(x,z) \boldsymbol{C} \\ &\quad \Big[\boldsymbol{D}_\Omega \Big(F_s(x,z) \boldsymbol{I} \Big) \Big] d\Omega \Big) N_j(y) \Big) dy + \\ &\quad \int_l \Big(\boldsymbol{D}_y^T \Big(N_i(y) \boldsymbol{I} \Big) \Big(\int_\Omega F_\tau(x,z) \boldsymbol{C} \\ &\quad F_s(x,z) d\Omega \Big) \boldsymbol{D}_y \Big(N_j(y) \boldsymbol{I} \Big) \Big) dy \Bigg\} \mathbf{q}_{sj} \end{aligned} \tag{14}$$

where Ω is the cross-section domain. The components of $\boldsymbol{C}$ are the material coefficients whose explicit expressions are not reported, see [47]. Differential operators arrays are given in Appendix B. The variation of the internal work is then written by means of the CUF fundamental nucleus,

$$\delta L_{int} = \delta \mathbf{q}_{\tau i}^T \mathbf{K}^{ij\tau s} \mathbf{q}_{sj} \tag{15}$$

$\mathbf{K}^{ij\tau s}$ is the stiffness matrix in the form of the fundamental nucleus. The explicit forms of the 9 components of $\mathbf{K}^{ij\tau s}$ are given in Appendix C.

No assumptions on the approximation order were made to obtain the fundamental nucleus. It is therefore possible to obtain refined 1D models without changing the formal expression of the nucleus components. This is the key-point of CUF which permits, with only nine FORTRAN statements, to implement theories of any-order.

The work of the external forces, δL_{ext} can be expressed as

$$\delta L_{ext} = \int_V \delta \boldsymbol{u}^T \tilde{\boldsymbol{F}} dV = \\ = \delta \mathbf{q}_{\tau i}^T \int_V N_i(y) F_\tau(x,z) \tilde{\boldsymbol{F}} dV \\ = \delta \mathbf{q}_{\tau i}^T \mathbf{P}^{\tau i} \tag{16}$$

where $\tilde{\boldsymbol{F}}$ is the generic load and $\mathbf{P}^{\tau i}$ is the vector of the nodal forces.

The global stiffness loading and unknowns arrays can be indicated as $\tilde{\mathbf{K}}$, $\tilde{\mathbf{F}}$ and $\mathbf{q}$, respectively. The following linear algebraic system has to be solved:

$$\tilde{\mathbf{K}} \mathbf{q} = \tilde{\mathbf{P}} \tag{17}$$

Shear locking correction is carried out by means of selective integration as shown in [28, 30]

3.2. 2D-shell finite elements

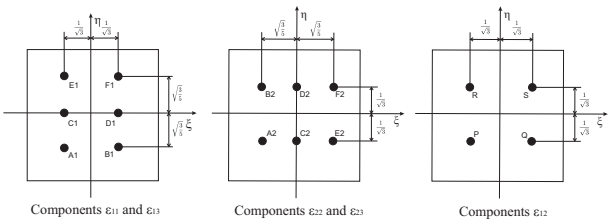

Figure 2. MITC9 tying points

MITC9 shell elements were formulated by using an interpolation of strain components within each element using a specific interpolation strategy for each component. The corresponding interpolation points, namely the *tying points*, are shown in Fig. 2 for the MITC9 shell element. MITC main arrays and geometrical relations are given in Appendix D.

The PVD for a shell can be expressed as

$$\int_V (\delta \boldsymbol{\varepsilon}_{pG}^T \boldsymbol{\sigma}_{pC} + \delta \boldsymbol{\varepsilon}_{nG}^T \boldsymbol{\sigma}_{nC}) dV = \delta L_e, \tag{18}$$

where V is the volume of the shell and T indicate the transposition operator. G and C indicate geometrical and constitutive relations, respectively. Constitutive equations can be written as follows:

$$\begin{aligned} \boldsymbol{\sigma}_{pC} &= \boldsymbol{\sigma}_{p_{jn}}^s = \boldsymbol{C}_{pp} \, \boldsymbol{\varepsilon}_{p_{jn}}^s + \boldsymbol{C}_{pn} \, \boldsymbol{\varepsilon}_{n_{jn}}^s \\ \boldsymbol{\sigma}_{nC} &= \boldsymbol{\sigma}_{n_{jn}}^s = \boldsymbol{C}_{np} \, \boldsymbol{\varepsilon}_{p_{jn}}^s + \boldsymbol{C}_{nn} \, \boldsymbol{\varepsilon}_{n_{jn}}^s \end{aligned} \tag{19}$$

By exploiting the geometrical relations and CUF, the PVD becomes

$$\int_V \delta \boldsymbol{q}_{\tau_i}^T [F_\tau \boldsymbol{C}_{3_{im}}^T (\boldsymbol{C}_{pp} \, F_s \boldsymbol{C}_{3_{jn}} + \boldsymbol{C}_{pn} \, (F_s \boldsymbol{C}_{1_{jn}} + F_{s_{,z}} \boldsymbol{C}_{2_{jn}})) + \\ (F_\tau \boldsymbol{C}_{1_{im}} + F_{\tau_{,z}} \boldsymbol{C}_{2_{im}})^T (\boldsymbol{C}_{np} \, F_s \boldsymbol{C}_{3_{jn}} + \\ \boldsymbol{C}_{nn} \, (F_s \boldsymbol{C}_{1_{jn}} + F_{s_{,z}} \boldsymbol{C}_{2_{jn}})] \boldsymbol{q}_{s_j} dV = \\ \int_V \delta \boldsymbol{q}_{\tau_i}^T F_\tau N_i \tilde{\boldsymbol{F}} \, dV \,, \tag{20}$$

By splitting the integrals in Equation 20, one has:

$$\begin{aligned}
&\delta \boldsymbol{q}_{\tau_i}^T \Big\{ \int_A F_\tau \Big(\int_\Omega [\boldsymbol{C}_{3_{im}}^T (\boldsymbol{C}_{pp} \boldsymbol{C}_{3_{jn}} + \boldsymbol{C}_{pn} \boldsymbol{C}_{1_{jn}}) + \boldsymbol{C}_{1_{im}}^T (\boldsymbol{C}_{np} \boldsymbol{C}_{3_{jn}} + \\
&\boldsymbol{C}_{nn} \boldsymbol{C}_{1_{jn}})] d\Omega \Big) F_{s_z} H \, dz \Big\} \boldsymbol{q}_{s_j} + \\
&\delta \boldsymbol{q}_{\tau_i}^T \Big\{ \int_A F_\tau \Big(\int_\Omega [(\boldsymbol{C}_{3_{im}}^T \boldsymbol{C}_{pn} + \boldsymbol{C}_{1_{im}}^T \boldsymbol{C}_{nn}) \boldsymbol{C}_{2_{jn}}] d\Omega \Big) F_{s_z} H \, dz \Big\} \boldsymbol{q}_{s_j} + \\
&\delta \boldsymbol{q}_{\tau_i}^T \Big\{ \int_A F_{\tau_z} \Big(\int_\Omega [\boldsymbol{C}_{2_{im}}^T (\boldsymbol{C}_{np} \boldsymbol{C}_{3_{jn}} + \boldsymbol{C}_{nn} \boldsymbol{C}_{1_{jn}})] d\Omega \Big) F_s H \, dz \Big\} \boldsymbol{q}_{s_j} + \\
&\delta \boldsymbol{q}_{\tau_i}^T \Big\{ \int_A F_{\tau_z} \Big(\int_\Omega [\boldsymbol{C}_{2_{im}}^T \boldsymbol{C}_{nn} \boldsymbol{C}_{2_{jn}}] d\Omega \Big) F_{s_z} H \, dz \Big\} \boldsymbol{q}_{s_j} = \\
&\delta \boldsymbol{q}_{\tau_i}^T \Big\{ \int_A F_\tau \Big(\int_\Omega N_i \tilde{\boldsymbol{F}} \, d\Omega \Big) H \, dz \Big\},
\end{aligned} \tag{21}$$

where $dV = H \, d\Omega \, dz$ is considered, A indicates the integration domain in the z direction and Ω is the in-plane integration domain. The variation of the internal work is then written by means of the CUF fundamental nucleus and the stiffness matrix in the form of the fundamental nucleus is obtained as in the 1D case,

$$\delta L_{int} = \delta \mathbf{q}_{\tau i}^T \mathbf{K}^{ij\tau s} \mathbf{q}_{sj} \tag{22}$$

The explicit forms of the 9 components of $\mathbf{K}^{ij\tau s}$ are given in Appendix C.

4. Results and Discussion

Numerical examples are presented and discussed in this section. First, results from preliminary assessments are shown where insights about convergence studies and locking are provided. Two well-known problems for thin walled structures are then investigated. In particular, the pinched shell and the Scordelis-Lo roof problems are considered.

4.1. 1D elements preliminary assessments

A cantilevered C-section beam was considered for this section in order to provide preliminary assessments including convergence analyses and comparisons with solid element models. The structural model considered was retrieved from [37]. The cross-section geometry is shown in Fig. 3. The length-to-height ratio, L/h, is equal to 20; the height-to-thickness ratio, h/t, is equal to 10 with h and b_2 equal to 1 [m] and $b_1 = b_2/2$. Two point loads were applied at [0, L, ±0.4] with $F_z = \mp 1$ [N]. The L9 distribution is shown in Fig. 4. The 9 L9 distribution presents refinements in the proximity of the loading points.

Table 1 shows the vertical displacement, u_z, of the point at [0, L, −0.5]. Solid, TE and LE model results are provided and the number of degrees of freedom (DOFs) are indicated for each model. The effect of the shear locking correction was also evaluated. Fig. 5 shows the 3D deformed configuration obtained by means of LE. These results suggest the following:

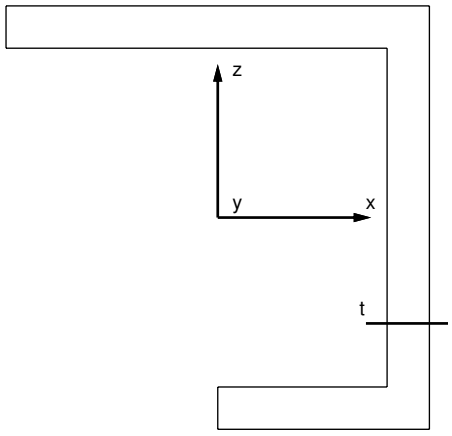

Figure 3. C-Section geometry

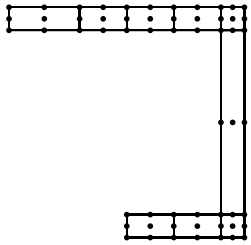

Figure 4. Cross-Section L9 distribution for the C-section beam

Table 1
Vertical displacement, u_z, at [0, L, −0.5], C-section beam

	DOFs	$u_z \times 10^8$, m
SOLID	84600	2.880
	1D TE	
EBBT	155	0.0
$N = 4$	1395	1.524
$N = 11$	7254	2.460
$N = 11^*$	7254	2.398
	1D LE	
9 L9, Fig. 4	5301	2.847
9 L9*, Fig. 4	5301	2.758

* without shear locking correction

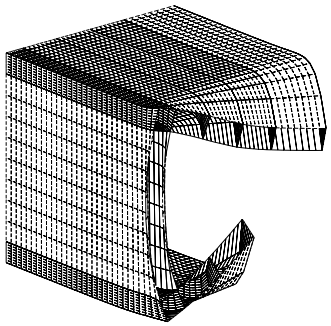

Figure 5. 3D deformed configuration of the C-shaped beam

1. Classical models, such as EBBT, cannot provide any cross-section distortion since they only account for constant cross-section in-plane displacements.
2. Higher-order TE models are able to qualitatively provide the distortion of the cross-section; however, expansion orders higher than 11 should be used to detect the solid solution.
3. LE models match the solid model solution with high accuracy and considerably lower computational costs.
4. Shear locking slightly affects present higher-order models. Its effects on the transverse displacement is of about 3%.

4.2. 2D elements preliminary assessments

Preliminary assessments were carried out by means of shell elements in order to provide mesh convergence studies and insights into shear and membrane locking phenomena and their correction. A pinched shell problem was chosen as a first numerical example. Material and geometrical data were retrieved from [48] where exact solutions based on CLT were also provided.

Table 2
Pinched shell physical data

Young's modulus	E	3×10^6 *psi*
Poisson's ratio	ν	0.3
Load	P	1 *lb*
Length	L	600 *in*
Radius	R	300 *in*
Thickness	t	3 *in*

Geometrical and material characteristics related to this problem are given in Fig. 6 and Table 2. Due to geometrical and loading symmetries, an eighth of the cylinder was modeled by means of Q9 elements and different shell models.

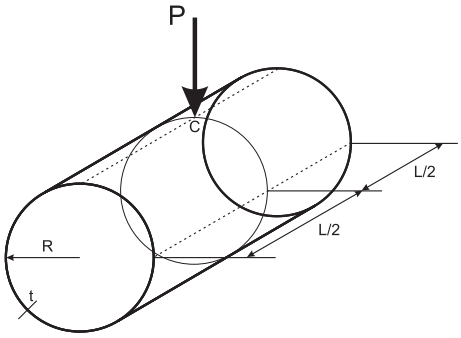

Figure 6. Pinched shell

Table 3
Simply-supported pinched shell, transversal displacement, $u_z \times 10^5$ *in*, at the loading point (midsurface)

Mesh	10×10	13×13
$u_{z_{ref}} = 1.8248$		
CLT	1.8230	1.8251
FSDT	1.8363	1.8396
ESL1	1.9582	1.9615
ESL2	1.8359	1.8406
ESL3	1.8379	1.8427
ESL4	1.8379	1.8427

Table 4
Clamped-clamped pinched shell, transversal displacement, $u_z \times 10^5$ *in*, at the loading point (midsurface)

Mesh	10×10	13×13
CLT	1.5097	1.5118
FSDT	1.5229	1.5262
ESL1	1.6114	1.6150
ESL2	1.5209	1.5258
ESL3	1.5228	1.5279
ESL4	1.5228	1.5279

Simply-supported and clamped-clamped boundary conditions were adopted and results are given in Tables 3 and 4, respectively. Higher-order shell theories are indicated with the acronym ESLN, where N is the order of expansion. The transverse displacement was evaluated at the midsurface of the loading point. In the simply-supported case, the reference value retrieved from [48] is indicated. The influence

of the Q9 mesh is shown for different shell models. No further improvements in the solution were provided by more refined meshes than 13×13. Classical (CLT and FSDT) and higher-order (up to the fourth-order) shell models were accounted for. The following statements hold:

1. An excellent agreement with the exact solution was obtained.

2. An ESL3 model is required to detect converged results. This model provides slightly higher displacement values than classical models.

The Scordelis-Lo roof problem [49] was investigated as a further preliminary assessment. Geometrical and material characteristics related to this problem are given in Fig. 7 and Table 5.

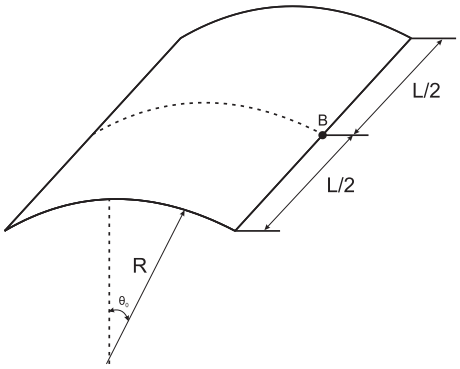

Figure 7. Scordelis-Lo barrel roof

Table 5
Roof physical data

Young's modulus	E	4.32×10^8 lb/ft^2
Poisson's ratio	ν	0.0
Load	P	90 lb/ft^2
Length	L	50 ft
Radius	R	25 ft
Thickness	t	0.25 ft
Angle	θ_0	$2\pi/9$ rad

Due to symmetric geometrical and loading conditions, a quarter of the structure was investigated. Geometrical boundary conditions were applied at the free tips and two BCs sets were accounted for, simply-supported and clamped-clamped.
Tables 6 and 7 show the transverse displacement of Point B for different shell models and Q9 meshes.

Table 6
Simply-supported roof, transversal displacement, u_z ft, at point B (midsurface)

Theory	13×13	16×16	20×20
	$u_{z_{ref}} = 0.3024$		
CLT	0.30057	0.30057	0.30057
FSDT	0.30091	0.30097	0.30104
FSDT*	0.30063	0.30083	0.30098
ESL1	0.30091	0.30097	0.30104
ESL2	0.30091	0.30097	0.30104
ESL3	0.30091	0.30097	0.30104
ESL4	0.30091	0.30097	0.30104

* without membrane and shear locking corrections

Table 7
Clamped-clamped roof, transversal displacement, u_z ft, at point B (midsurface)

Theory	13×13	16×16	20×20
FSDT	0.14852	0.14855	0.14858
ESL1	0.14852	0.14855	0.14858
ESL2	0.14852	0.14855	0.14858
ESL3	0.14852	0.14855	0.14858
ESL4	0.14852	0.14855	0.14858

* without membrane and shear locking corrections

In the simply-supported case, a reference exact value is also indicated, this value was retrieved from [49] and it was obtained by means of a CLT model. Furthermore, the influence of the shear and membrane locking corrections were evaluated in the simply-supported case. The results obtained suggest the following:

1. A 20×20 Q9 mesh ensures high accuracy for the detection of the transverse displacement.

2. For this problem, higher-order shell models do not provide an improvement over the classical models solution.

3. The influence of locking is very low.

4. The difference between the present CLT solution and the one in [49] is due to the geometrical assumptions made in the paper by Scordelis and Lo. These assumptions were not adopted in the present formulation.

Further analyses were carried out to highlight locking phenomena. Lower thickness and load values were considered, $t = 0.0025$ [ft] and $P = 0.09$ [lb/ft^2]. Results for the simply-supported case are given in Table 8. It can be stated that

1. As expected, for very thin shell structures locking phenomena are extremely important.

2. Locking corrections are mandatory.

Table 8
Simply-supported roof, transversal displacement, u_z ft, at point B (midsurface), $t = 0.0025$ ft, $P = 0.09$ lb/ft^2

Theory	13×13	16×16	20×20
FSDT	3.251	3.257	3.260
FSDT*	0.893	1.278	1.802
FSDT**	0.973	1.325	1.827

* without membrane and shear locking corrections
** without membrane locking corrections

3. Both lockings (membrane and shear) play an important role, however in the problems considered, membrane locking is predominant.

4.3. 1D and 2D models solutions for pinched shell

This section deals with the comparison of the results provided by 1D and 2D models for the pinched shell model. The characteristics of the structural problem are the same as those seen previously. The LE class was used for 1D models since TE needs very high expansion orders to provide satisfactory accuracies when point loads are applied to thin walled structures, as shown in [37]. Fig. 8 shows

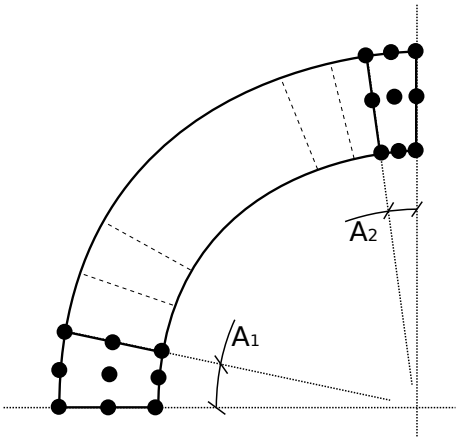

Figure 8. Cross-section L-elements distribution for the pinched shell

the cross-section L-element distribution adopted in the 1D model. For the sake of brevity, only L9 elements are shown. Two different distributions were used. In the first configuration, 29 L9 elements were considered and a uniform mesh was adopted ($A_1/A_2 = 1$). In the second configuration, 30 L16 elements were adopted and the element distribution was linearly refined in proximity to the loading point ($A_1/A_2 = 10$).
Tables 9 and 10 present the transverse displacement of the loading point for the simply-supported and the clamped-clamped case, respectively.

Table 9
Simply-supported pinched shell, transversal displacement, u_z, at the loading point (midsurface)

Model	$u_z \times 10^5$, in	DOFs
	2D shell	
ESL3	1.8427	8748
	1D LE	
29 L9	1.7959	5310
30 L16	1.8359	10920

Table 10
Clamped-clamped pinched shell, transversal displacement, u_z, at the loading point (midsurface)

Model	$u_z \times 10^5$, in	DOFs
	2D shell	
ESL3	1.5279	8748
	1D LE	
30 L16	1.5196	10920

The number of DOFs of each model is reported in the last column, an eighth of the structure was considered. Fig. 9 shows the deformed top-half cross-section at $L/2$.

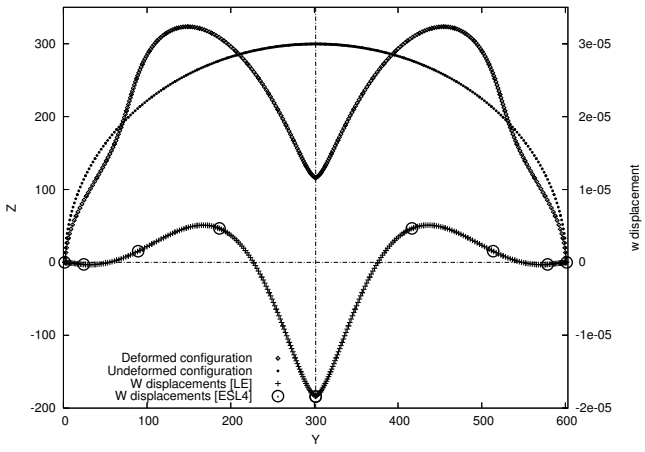

Figure 9. Simply-supported pinched shell, comparisons between ESL4 and LE at the midspan section

The distribution of the transverse displacement is shown on the same plot. Fig. 10 shows the 3D deformed configuration of a half shell by means of the LE model. The results obtained suggest the following:

1. A very good agreement was found between beam and shell solutions.

2. L16 cross-section elements are needed to provide satisfactory accuracy.

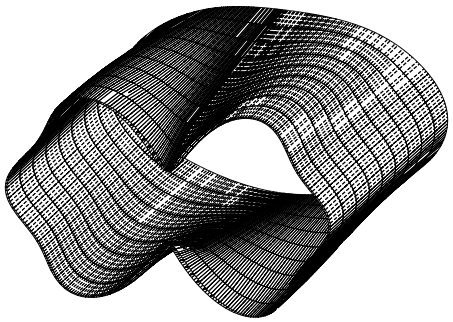

Figure 10. Simply-supported pinched shell, 3D deformed configuration by the 30 L16 model

3. The present 1D formulation is able to detect very complex 3D deformed configurations of thin walled structures undergoing point loads with computational costs comparable to those of shell models.

4.4. 1D and 2D model solutions for the Scordelis-Lo roof problem

The Scordelis-Lo roof problem is investigated in this section to compare results from beam and shell models. The characteristics of the structural problem are the same as those seen previously.

Table 11
Simply-supported barrel vault, transversal displacement at point B (midsurface)

Model	u_z, ft	DOFs
	2D shell	
FSDT	0.30104	8405
	1D TE	
$N = 1$	0.01869	549
$N = 2$	0.02631	1098
$N = 3$	0.11364	1830
$N = 4$	0.25127	2745
$N = 5$	0.30335	3843

The TE class was adopted for 1D models. Tables 11 and 12 show the transverse displacement of point B (see Fig. 7) for simply-supported and clamped-clamped BCs, respectively. Shell and different refined beam models were accounted for. The 3D deformed configuration of the roof is shown in Fig. 11 where the $N = 5$ solution is given. It can be stated that

1. The 1D model matches the shell solution perfectly.

Table 12
Clamped-clamped barrel vault, transversal displacement at point B (midsurface)

Model	u_z, ft	DOFs
	2D shell	
FSDT	0.14858	8405
	1D TE	
$N = 1$	0.00493	549
$N = 2$	0.00884	1098
$N = 3$	0.07367	1830
$N = 4$	0.13976	2745
$N = 5$	0.14855	3843

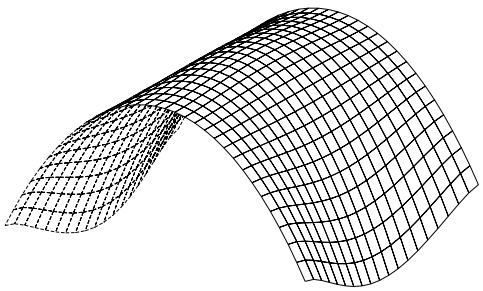

Figure 11. Simply supported Barrel vault deformation, 1D TE, $N = 5$

2. An $N = 5$ model is needed to detect the shell model accuracy, models up to the third-order ($N = 3$) provide completely wrong results.

3. The 3D deformed configuration is well described by the refined 1D model.

4. In this case computational costs of 1D models are considerably lower than those of shell models.

Further investigations were carried out to analyze locking phenomena. Lower thickness and load values were considered, $t = 0.0025$ [ft] and $P = 0.09$ [lb/ft^2]. Results for the clamped-clamped case are given in Tables 13. It is important to underline that, in the 1D case, only the shear locking is corrected while membrane locking does not affect the solution. An $N = 9$ was chosen after a convergence study. It can be stated that

1. As expected, for very thin shell structures locking phenomena are extremely important for shells.

2. Higher-order 1D models by CUF are not affected by numerical locking.

Table 13
Clamped-clamped roof, transversal displacement, u_z, at point B (midsurface), $t = 0.0025\ ft$, $P = 0.09\ lb/ft^2$

Theory	u_z, ft	DOFs
	2D shell	
FSDT	−1.446	8405
FSDT*	−0.796	8405
	1D TE	
$N = 9$	−1.461	10065
$N = 9$**	−1.462	10065

* without membrane and shear locking corrections
** without shear locking correction

3. The thinner the structure, the higher the 1D model order needed to detect the shell solution. Consequently, 1D models computational costs increase if very thin structures are considered.

5. Conclusions

The structural analysis of isotropic thin walled structures has been presented in this paper. Typical shell problems have been assessed by means of refined beam (1D) models. Shell (2D) finite elements based on refined theories have been exploited for comparison purposes. Higher-order models and related finite elements have been built in the framework of the Carrera Unified Formulation (CUF). In CUF, problem matrices and vectors can be obtained by means of a unified formulation which is independent of the order of the structural model. Also, 1D and 2D formulations can be easily obtained by acting on geometrical relations and expansion functions. The Principle of Virtual Displacements has been exploited.
Two classes of 1D theories have been employed, namely TE and LE classes. TE is based on Taylor-like polynomials; LE is based on Lagrange polynomials defined above discretized portions of the cross-section. Taylor-like polynomials have also been exploited to implement refined shell models, nine-node MITC finite elements have been adopted.
Different thin walled structures have been considered, such as C-section beams, pinched shells and the Scordelis-Lo roof. Results obtained from present beam and shell models have been compared with those from 3D finite elements and exact solutions from open literature. The effect of numerical locking has also been evaluated. The following conclusions can be drawn:

1. In general, an excellent agreement was found between the present formulation, 3D finite elements and results reported in literature.

2. The proposed higher-order 1D formulation is able to detect shell solutions. If thin structures undergoing distributed loads are considered, computational costs of 1D CUF models will be considerably lower than shells. On the other hand, in the case of very thin structures or point loads, 1D and shell computational costs are similar.

3. In the case of 1D CUF models, it can be stated that the LE class should be used to analyze point load problems and TE should be used if distributed loads are considered.

4. Another important advantage of 1D CUF is that it is barely affected by numerical locking which can, however, dramatically affect the accuracy of shell elements.

5. The unified formulation by Carrera represents a reliable tool to deal with 1D and 2D refined models and a wide variety of modeling approaches.

Future works should deal with further comparative studies on composite structures and free vibration problems.

A. Differential Operators and Material Matrices for CUF shells

The strain-displacement relations are given by the linear part of the *3D Green Lagrange strain tensor*,

$$\begin{aligned}
\varepsilon_{\alpha\alpha} &= F_\tau u_{\tau,\alpha} \\
\varepsilon_{\beta\beta} &= F_\tau\Big[(1+\frac{z}{R})\frac{w_\tau}{R} + (1+\frac{z}{R})v_{\tau,\beta}\Big] \\
\varepsilon_{\alpha\beta} &= F_\tau\Big[u_{\tau,\beta} + (1+\frac{z}{R})v_{\tau,\alpha}\Big] \\
\varepsilon_{\alpha z} &= w_{\tau,\alpha}F_\tau + u_\tau F_{\tau,z} \\
\varepsilon_{\beta z} &= F_\tau\Big[w_{\tau,\beta} - \frac{v_\tau}{R}\Big] + F_{\tau,z}\Big[(1+\frac{z}{R})v_\tau\Big] \\
\varepsilon_{zz} &= w_\tau F_{\tau,z}
\end{aligned} \tag{23}$$

where the cylindrical shell assumptions are adopted. More details can be found in [25, 27]. Geometrical relations can be expressed in matrix form as

$$\begin{aligned}
\boldsymbol{\varepsilon}_p &= (\boldsymbol{D}_p + \boldsymbol{A}_p)\boldsymbol{u} \\
\boldsymbol{\varepsilon}_n &= (\boldsymbol{D}_{n\Omega} + \boldsymbol{D}_{nz} - \boldsymbol{A}_n)\boldsymbol{u}
\end{aligned} \tag{24}$$

where subscripts (p) and (n) indicate in-plane and normal components, respectively. The differential operators for shells are

$$\boldsymbol{D}_p = \begin{bmatrix} \partial_\alpha & 0 & 0 \\ 0 & H\partial_\beta & 0 \\ \partial_\beta & H\partial_\alpha & 0 \end{bmatrix}, \quad \boldsymbol{D}_{n\Omega} = \begin{bmatrix} 0 & 0 & \partial_\alpha \\ 0 & 0 & \partial_\beta \\ 0 & 0 & 0 \end{bmatrix},$$

$$\boldsymbol{D}_{nz} = \partial_z \cdot \boldsymbol{A}_{nz} = \partial_z \begin{bmatrix} 1 & 0 & 0 \\ 0 & H & 0 \\ 0 & 0 & 1 \end{bmatrix},$$

$$\boldsymbol{A}_p = \begin{bmatrix} 0 & 0 & 0 \\ 0 & 0 & \frac{1}{R}H \\ 0 & 0 & 0 \end{bmatrix}, \boldsymbol{A}_n = \begin{bmatrix} 0 & 0 & 0 \\ 0 & \frac{1}{R} & 0 \\ 0 & 0 & 0 \end{bmatrix},$$

and

$$H = (1 + \frac{z}{R})$$

Material coefficient arrays are

$$\boldsymbol{C}_{pp} = \begin{bmatrix} C_{11} & C_{12} & C_{16} \\ C_{12} & C_{22} & C_{26} \\ C_{16} & C_{26} & C_{66} \end{bmatrix} \qquad \boldsymbol{C}_{pn} = \begin{bmatrix} 0 & 0 & C_{13} \\ 0 & 0 & C_{23} \\ 0 & 0 & C_{36} \end{bmatrix}$$

$$\boldsymbol{C}_{np} = \begin{bmatrix} 0 & 0 & 0 \\ 0 & 0 & 0 \\ C_{13} & C_{23} & C_{36} \end{bmatrix} \qquad \boldsymbol{C}_{nn} = \begin{bmatrix} C_{55} & C_{45} & 0 \\ C_{45} & C_{44} & 0 \\ 0 & 0 & C_{33} \end{bmatrix}$$

B. Differential Operators for CUF 1D

Linear strain-displacement relations are used,

$$\boldsymbol{\epsilon} = \boldsymbol{D}\mathbf{u} = (\boldsymbol{D}_y + \boldsymbol{D}_\Omega)\mathbf{u}$$

where

$$\boldsymbol{D} = \begin{bmatrix} \frac{\partial}{\partial x} & 0 & 0 \\ 0 & \frac{\partial}{\partial y} & 0 \\ 0 & 0 & \frac{\partial}{\partial z} \\ \frac{\partial}{\partial y} & \frac{\partial}{\partial x} & 0 \\ \frac{\partial}{\partial z} & 0 & \frac{\partial}{\partial x} \\ 0 & \frac{\partial}{\partial z} & \frac{\partial}{\partial y} \end{bmatrix} = \begin{bmatrix} \frac{\partial}{\partial x} & 0 & 0 \\ 0 & 0 & 0 \\ 0 & 0 & \frac{\partial}{\partial z} \\ 0 & \frac{\partial}{\partial x} & 0 \\ \frac{\partial}{\partial z} & 0 & \frac{\partial}{\partial x} \\ 0 & \frac{\partial}{\partial z} & 0 \end{bmatrix} + \begin{bmatrix} 0 & 0 & 0 \\ 0 & \frac{\partial}{\partial y} & 0 \\ 0 & 0 & 0 \\ \frac{\partial}{\partial y} & 0 & 0 \\ 0 & 0 & 0 \\ 0 & 0 & \frac{\partial}{\partial y} \end{bmatrix} = [\boldsymbol{D}_\Omega] + [\boldsymbol{D}_y]$$

C. Fundamental Nucleus Components

The nine components of the beam stiffness matrix fundamental nucleus are defined as:

$$\begin{aligned} K_{xx}^{ij\tau s} = {} & \tilde{C}_{22} \int_\Omega F_{\tau,x} F_{s,x} d\Omega \int_l N_i N_j dy + \\ & \tilde{C}_{66} \int_\Omega F_\tau F_s d\Omega \int_l N_{i,y} N_{j,y} dy + \\ & \tilde{C}_{44} \int_\Omega F_{\tau,z} F_{s,z} d\Omega \int_l N_i N_j dy + \\ & \tilde{C}_{26} \int_\Omega F_{\tau,x} F_s d\Omega \int_l N_i N_{j,y} dy + \\ & \tilde{C}_{26} \int_\Omega F_\tau F_{s,x} d\Omega \int_l N_{i,y} N_j dy \end{aligned}$$

$$\begin{aligned} K_{xy}^{ij\tau s} = {} & \tilde{C}_{66} \int_\Omega F_\tau F_{s,x} d\Omega \int_l N_{i,y} N_j dy + \\ & \tilde{C}_{45} \int_\Omega F_{\tau,z} F_{s,z} d\Omega \int_l N_i N_j dy + \\ & \tilde{C}_{23} \int_\Omega F_{\tau,x} F_s d\Omega \int_l N_i N_{j,y} dy + \\ & \tilde{C}_{36} \int_\Omega F_\tau F_s d\Omega \int_l N_{i,y} N_{j,y} dy + \\ & \tilde{C}_{26} \int_\Omega F_{\tau,x} F_{s,x} d\Omega \int_l N_i N_j dy \end{aligned}$$

$$\begin{aligned} K_{xz}^{ij\tau s} = {} & \tilde{C}_{45} \int_\Omega F_{\tau,z} F_s d\Omega \int_l N_i N_{j,y} dy + \\ & \tilde{C}_{12} \int_\Omega F_{\tau,x} F_{s,z} d\Omega \int_l N_i N_j dy + \\ & \tilde{C}_{16} \int_\Omega F_\tau F_{s,z} d\Omega \int_l N_{i,y} N_j dy + \\ & \tilde{C}_{44} \int_\Omega F_{\tau,z} F_{s,x} d\Omega \int_l N_i N_j dy \end{aligned}$$

$$\begin{aligned} K_{yx}^{ij\tau s} = {} & \tilde{C}_{66} \int_\Omega F_{\tau,x} F_s d\Omega \int_l N_i N_{j,y} dy + \\ & \tilde{C}_{45} \int_\Omega F_{\tau,z} F_{s,z} d\Omega \int_l N_i N_j dy + \\ & \tilde{C}_{23} \int_\Omega F_\tau F_{s,x} d\Omega \int_l N_{i,y} N_j dy + \\ & \tilde{C}_{36} \int_\Omega F_\tau F_s d\Omega \int_l N_{i,y} N_{j,y} dy + \\ & \tilde{C}_{26} \int_\Omega F_{\tau,x} F_{s,x} d\Omega \int_l N_i N_j dy \end{aligned}$$

$$\begin{aligned} K_{yy}^{ij\tau s} = {} & \tilde{C}_{66} \int_\Omega F_{\tau,x} F_{s,x} d\Omega \int_l N_i N_j dy + \\ & \tilde{C}_{36} \int_\Omega F_{\tau,x} F_s d\Omega \int_l N_i N_{j,y} dy + \\ & \tilde{C}_{36} \int_\Omega F_\tau F_{s,x} d\Omega \int_l N_{i,y} N_j dy + \\ & \tilde{C}_{55} \int_\Omega F_{\tau,z} F_{s,z} d\Omega \int_l N_i N_j dy + \\ & \tilde{C}_{33} \int_\Omega F_\tau F_s d\Omega \int_l N_{i,y} N_{j,y} dy \end{aligned}$$

$$\begin{aligned} K_{yz}^{ij\tau s} = {} & \tilde{C}_{45} \int_\Omega F_{\tau,z} F_{s,x} d\Omega \int_l N_i N_j dy + \\ & \tilde{C}_{55} \int_\Omega F_{\tau,z} F_s d\Omega \int_l N_i N_{j,y} dy + \\ & \tilde{C}_{13} \int_\Omega F_\tau F_{s,z} d\Omega \int_l N_{i,y} N_j dy + \\ & \tilde{C}_{16} \int_\Omega F_{\tau,x} F_{s,z} d\Omega \int_l N_i N_j dy \end{aligned}$$

$$\begin{aligned} K_{zx}^{ij\tau s} = {} & \tilde{C}_{45} \int_\Omega F_\tau F_{s,z} d\Omega \int_l N_{i,y} N_j dy + \\ & \tilde{C}_{12} \int_\Omega F_{\tau,z} F_{s,x} d\Omega \int_l N_i N_j dy + \\ & \tilde{C}_{16} \int_\Omega F_{\tau,z} F_s d\Omega \int_l N_i N_{j,y} dy + \\ & \tilde{C}_{44} \int_\Omega F_{\tau,x} F_{s,z} d\Omega \int_l N_i N_j dy \end{aligned}$$

$$\begin{aligned} K_{zy}^{ij\tau s} = {} & \tilde{C}_{45} \int_\Omega F_{\tau,x} F_{s,z} d\Omega \int_l N_i N_j dy + \\ & \tilde{C}_{55} \int_\Omega F_\tau F_{s,z} d\Omega \int_l N_{i,y} N_j dy + \\ & \tilde{C}_{13} \int_\Omega F_{\tau,z} F_s d\Omega \int_l N_i N_{j,y} dy + \\ & \tilde{C}_{16} \int_\Omega F_{\tau,z} F_{s,x} d\Omega \int_l N_i N_j dy \end{aligned}$$

$$
\begin{aligned}
K_{zz}^{ijts} = \; & \tilde{C}_{55} \int_\Omega F_\tau F_s d\Omega \int_l N_{i,y} N_{j,y} dy + \\
& \tilde{C}_{11} \int_\Omega F_{\tau,z} F_{s,z} d\Omega \int_l N_i N_j dy + \\
& \tilde{C}_{45} \int_\Omega F_\tau F_{s,x} d\Omega \int_l N_{i,y} N_j dy + \\
& \tilde{C}_{45} \int_\Omega F_{\tau,x} F_s d\Omega \int_l N_i N_{j,y} dy + \\
& \tilde{C}_{44} \int_\Omega F_{\tau,x} F_{s,x} d\Omega \int_l N_i N_j dy
\end{aligned}
$$

The explicit form of the shell fundamental nucleus is the following:

$$
\begin{aligned}
K_{11}^{\tau sij} = \; & C_{55} N_{i,\alpha_{m1}} \lhd N_{m1} N_{n1} \rhd_\Omega N_{j,\alpha_{n1}} \lhd F_{\tau,z} F_{s,z} \rhd_A + \\
& C_{11} N_{i,\alpha_{m1}} \lhd N_{m1} N_{n1} \rhd_\Omega N_{j,\alpha_{n1}} \lhd F_\tau F_s \rhd_A + \\
& C_{16} N_{i,\beta_{m3}} \lhd N_{m3} N_{n1} \rhd_\Omega N_{j,\alpha_{n1}} \lhd F_\tau F_s \rhd_A + \\
& C_{16} N_{i,\alpha_{m1}} \lhd N_{m1} N_{n3} \rhd_\Omega N_{j,\beta_{n3}} \lhd F_\tau F_s \rhd_A + \\
& C_{66} N_{i,\beta_{m3}} \lhd N_{m3} N_{n3} \rhd_\Omega N_{j,\beta_{n3}} \lhd F_\tau F_s \rhd_A
\end{aligned}
$$

$$
\begin{aligned}
K_{12}^{\tau sij} = \; & -C_{45} \tfrac{1}{R} N_{i_{m1}} \lhd N_{m1} N_{n2} \rhd_\Omega N_{j_{n2}} \lhd F_{\tau,z} F_s \rhd_A + \\
& C_{45} N_{i_{m1}} \lhd N_{m1} N_{n2} \rhd_\Omega N_{j_{n2}} \lhd H F_{\tau,z} F_{s,z} \rhd_A + \\
& C_{12} N_{i,\alpha_{m1}} \lhd N_{m1} N_{n2} \rhd_\Omega N_{j,\beta_{n2}} \lhd H F_\tau F_s \rhd_A + \\
& C_{16} N_{i,\alpha_{m1}} \lhd N_{m1} N_{n3} \rhd_\Omega N_{j,\alpha_{n3}} \lhd H F_\tau F_s \rhd_A + \\
& C_{26} N_{i,\beta_{m3}} \lhd N_{m3} N_{n2} \rhd_\Omega N_{j,\beta_{n2}} \lhd H F_\tau F_s \rhd_A + \\
& C_{66} N_{i,\beta_{m3}} \lhd N_{m3} N_{n3} \rhd_\Omega N_{j,\alpha_{n3}} \lhd H F_\tau F_s \rhd_A
\end{aligned}
$$

$$
\begin{aligned}
K_{13}^{\tau sij} = \; & C_{13} N_{i,\alpha_{m1}} \lhd N_{m1} N_j \rhd_\Omega \lhd F_\tau F_{s,z} \rhd_A + \\
& C_{36} N_{i,\beta_{m3}} \lhd N_{m3} N_j \rhd_\Omega \lhd F_\tau F_{s,z} \rhd_A + \\
& C_{12} \tfrac{1}{R} N_{i,\alpha_{m1}} \lhd N_{m1} N_{n2} \rhd_\Omega N_{j_{n2}} \lhd H F_\tau F_s \rhd_A + \\
& C_{26} \tfrac{1}{R} N_{i,\beta_{m3}} \lhd N_{m3} N_{n2} \rhd_\Omega N_{j_{n2}} \lhd H F_\tau F_s \rhd_A + \\
& C_{55} N_{i_{m1}} \lhd N_{m1} N_{n1} \rhd_\Omega N_{j,\alpha_{n1}} \lhd F_{\tau,z} F_s \rhd_A + \\
& C_{45} N_{i_{m1}} \lhd N_{m1} N_{n2} \rhd_\Omega N_{j,\beta_{n2}} \lhd F_{\tau,z} F_s \rhd_A
\end{aligned}
$$

$$
\begin{aligned}
K_{21}^{\tau sij} = \; & -C_{45} \tfrac{1}{R} N_{i_{m2}} \lhd N_{m2} N_{n1} \rhd_\Omega N_{j_{n1}} \lhd F_\tau F_{s,z} \rhd_A + \\
& C_{45} N_{i_{m2}} \lhd N_{m2} N_{n1} \rhd_\Omega N_{j_{n1}} \lhd H F_{\tau,z} F_{s,z} \rhd_A + \\
& C_{12} N_{i,\beta_{m2}} \lhd N_{m2} N_{n1} \rhd_\Omega N_{j,\alpha_{n1}} \lhd H F_\tau F_s \rhd_A + \\
& C_{16} N_{i,\alpha_{m3}} \lhd N_{m3} N_{n1} \rhd_\Omega N_{j,\alpha_{n1}} \lhd H F_\tau F_s \rhd_A + \\
& C_{26} N_{i,\beta_{m2}} \lhd N_{m2} N_{n3} \rhd_\Omega N_{j,\beta_{n3}} \lhd H F_\tau F_s \rhd_A + \\
& C_{66} N_{i,\alpha_{m3}} \lhd N_{m3} N_{n3} \rhd_\Omega N_{j,\beta_{n3}} \lhd H F_\tau F_s \rhd_A
\end{aligned}
$$

$$
\begin{aligned}
K_{22}^{\tau sij} = \; & C_{22} N_{i,\beta_{m2}} \lhd N_{m2} N_{n2} \rhd_\Omega N_{j,\beta_{n2}} \lhd H^2 F_\tau F_s \rhd_A + \\
& C_{26} N_{i,\beta_{m2}} \lhd N_{m2} N_{n3} \rhd_\Omega N_{j,\alpha_{n3}} \lhd H^2 F_\tau F_s \rhd_A \\
& C_{26} N_{i,\alpha_{m3}} \lhd N_{m3} N_{n2} \rhd_\Omega N_{j,\beta_{n2}} \lhd H^2 F_\tau F_s \rhd_A + \\
& C_{66} N_{i,\alpha_{m3}} \lhd N_{m3} N_{n3} \rhd_\Omega N_{j,\alpha_{n3}} \lhd H^2 F_\tau F_s \rhd_A + \\
& C_{44} \tfrac{1}{R^2} N_{i_{m2}} \lhd N_{m2} N_{n2} \rhd_\Omega N_{j_{n2}} \lhd F_\tau F_s \rhd_A - \\
& C_{44} \tfrac{1}{R} N_{i_{m2}} \lhd N_{m2} N_{n2} \rhd_\Omega N_{j_{n2}} \lhd H F_\tau F_{s,z} \rhd_A + \\
& -C_{44} \tfrac{1}{R} N_{i_{m2}} \lhd N_{m2} N_{n2} \rhd_\Omega N_{j_{n2}} \lhd H F_{\tau,z} F_s \rhd_A + \\
& C_{44} N_{i_{m2}} \lhd N_{m2} N_{n2} \rhd_\Omega N_{j_{n2}} \lhd H^2 F_{\tau,z} F_{s,z} \rhd_A
\end{aligned}
$$

$$
\begin{aligned}
K_{23}^{\tau sij} = \; & C_{22} \tfrac{1}{R} N_{i,\beta_{m2}} \lhd N_{m2} N_{n2} \rhd_\Omega N_{j_{n2}} \lhd H^2 F_\tau F_s \rhd_A + \\
& C_{23} N_{i,\beta_{m2}} \lhd N_{m2} N_j \rhd_\Omega \lhd H F_\tau F_{s,z} \rhd_A + \\
& C_{26} \tfrac{1}{R} N_{i,\alpha_{m3}} \lhd N_{m3} N_{n2} \rhd_\Omega N_{j_{n2}} \lhd H^2 F_\tau F_s \rhd_A + \\
& C_{36} N_{i,\alpha_{m3}} \lhd N_{m3} N_j \rhd_\Omega \lhd H F_\tau F_{s,z} \rhd_A + \\
& -C_{45} \tfrac{1}{R} N_{i_{m2}} \lhd N_{m2} N_{n1} \rhd_\Omega N_{j,\alpha_{n1}} \lhd F_\tau F_s \rhd_A - \\
& C_{44} \tfrac{1}{R} N_{i_{m2}} \lhd N_{m2} N_{n2} \rhd_\Omega N_{j,\beta_{n2}} \lhd F_\tau F_s \rhd_A + \\
& C_{45} N_{i_{m2}} \lhd N_{m2} N_{n1} \rhd_\Omega N_{j,\alpha_{n1}} \lhd H F_{\tau,z} F_s \rhd_A + \\
& C_{44} N_{i_{m2}} \lhd N_{m2} N_{n2} \rhd_\Omega N_{j,\beta_{n2}} \lhd H F_{\tau,z} F_s \rhd_A
\end{aligned}
$$

$$
\begin{aligned}
K_{31}^{\tau sij} = \; & C_{55} N_{i,\alpha_{m1}} \lhd N_{m1} N_{n1} \rhd_\Omega N_{j_{n1}} \lhd F_\tau F_{s,z} \rhd_A + \\
& C_{45} N_{i,\beta_{m2}} \lhd N_{m2} N_{n1} \rhd_\Omega N_{j_{n1}} \lhd F_\tau F_{s,z} \rhd_A + \\
& C_{12} \tfrac{1}{R} N_{i_{m2}} \lhd N_{m2} N_{n1} \rhd_\Omega N_{j,\alpha_{n1}} \lhd H F_\tau F_s \rhd_A + \\
& C_{13} \lhd N_i N_{n1} \rhd_\Omega N_{j,\alpha_{n1}} \lhd F_{\tau,z} F_s \rhd_A + \\
& C_{26} \tfrac{1}{R} N_{i_{m2}} \lhd N_{m2} N_{n3} \rhd_\Omega N_{j,\beta_{n3}} \lhd H F_\tau F_s \rhd_A + \\
& C_{36} \lhd N_i N_{n3} \rhd_\Omega N_{j,\beta_{n3}} \lhd F_{\tau,z} F_s \rhd_A
\end{aligned}
$$

$$
\begin{aligned}
K_{32}^{\tau sij} = \; & C_{22} \tfrac{1}{R} N_{i_{m2}} \lhd N_{m2} N_{n2} \rhd_\Omega N_{j,\beta_{n2}} \lhd H^2 F_\tau F_s \rhd_A + \\
& C_{23} \lhd N_i N_{n2} \rhd_\Omega N_{j,\beta_{n2}} \lhd H F_{\tau,z} F_s \rhd_A + \\
& C_{26} \tfrac{1}{R} N_{i_{m2}} \lhd N_{m2} N_{n3} \rhd_\Omega N_{j,\alpha_{n3}} \lhd H^2 F_\tau F_s \rhd_A + \\
& C_{36} \lhd N_i N_{n3} \rhd_\Omega N_{j,\alpha_{n3}} \lhd H F_{\tau,z} F_s \rhd_A + \\
& -C_{45} \tfrac{1}{R} N_{i,\alpha_{m1}} \lhd N_{m1} N_{n2} \rhd_\Omega N_{j_{n2}} \lhd F_\tau F_s \rhd_A - \\
& C_{44} \tfrac{1}{R} N_{i,\beta_{m2}} \lhd N_{m2} N_{n2} \rhd_\Omega N_{j_{n2}} \lhd F_\tau F_s \rhd_A + \\
& C_{45} N_{i,\alpha_{m1}} \lhd N_{m1} N_{n2} \rhd_\Omega N_{j_{n2}} \lhd H F_{\tau,z} F_{s,z} \rhd_A + \\
& C_{44} N_{i,\beta_{m2}} \lhd N_{m2} N_{n2} \rhd_\Omega N_{j_{n2}} \lhd H F_\tau F_s \rhd_A
\end{aligned}
$$

$$
\begin{aligned}
K_{33}^{\tau sij} = \; & C_{22} \tfrac{1}{R^2} N_{i_{m2}} \lhd N_{m2} N_{n2} \rhd_\Omega N_{j_{n2}} \lhd H^2 F_\tau F_s \rhd_A + \\
& C_{23} \tfrac{1}{R} N_{i_{m2}} \lhd N_{m2} N_j \rhd_\Omega \lhd H F_\tau F_{s,z} \rhd_A + \\
& C_{23} \tfrac{1}{R} \lhd N_i N_{n2} \rhd_\Omega N_{j_{n2}} \lhd H F_{\tau,z} F_s \rhd_A + \\
& C_{33} \lhd N_i N_j \rhd_\Omega \lhd F_{\tau,z} F_{s,z} \rhd_A + \\
& C_{55} N_{i,\alpha_{m1}} \lhd N_{m1} N_{n1} \rhd_\Omega N_{j,\alpha_{n1}} \lhd F_\tau F_s \rhd_A + \\
& C_{45} N_{i,\beta_{m2}} \lhd N_{m2} N_{n1} \rhd_\Omega N_{j,\alpha_{n1}} \lhd F_\tau F_s \rhd_A + \\
& C_{45} N_{i,\alpha_{m1}} \lhd N_{m1} N_{n2} \rhd_\Omega N_{j,\beta_{n2}} \lhd F_\tau F_s \rhd_A + \\
& C_{44} N_{i,\beta_{m2}} \lhd N_{m2} N_{n2} \rhd_\Omega N_{j,\beta_{n2}} \lhd F_\tau F_s \rhd_A
\end{aligned}
$$

where $\lhd \ldots \rhd_\Omega$ indicates $\int_\Omega \ldots d\Omega$ and $\lhd \ldots \rhd_A$ indicates $\int_A \ldots dz$ (A is the integration domain in the z direction).

D. MITC arrays

The interpolating functions are arranged in the following arrays:

$$
\begin{aligned}
N_{m1} &= [N_{A1}, N_{B1}, N_{C1}, N_{D1}, N_{E1}, N_{F1}] \\
N_{m2} &= [N_{A2}, N_{B2}, N_{C2}, N_{D2}, N_{E2}, N_{F2}] \\
N_{m3} &= [N_P, N_Q, N_R, N_S]
\end{aligned}
$$

From this point on, subscripts $m1$, $m2$ and $m3$ indicate the quantities calculated in the points $(A1, B1, C1, D1, E1, F1)$, $(A2, B2, C2, D2, E2, F2)$ and (P, Q, R, S), respectively. According to MITC method, the strains components are interpolated on tying points as follows:

$$\varepsilon_p = \begin{bmatrix}\varepsilon_{11}\\ \varepsilon_{22}\\ \varepsilon_{12}\end{bmatrix} = \begin{bmatrix}N_{m1} & 0 & 0\\ 0 & N_{m2} & 0\\ 0 & 0 & N_{m3}\end{bmatrix}\begin{bmatrix}\varepsilon_{11_{m1}}\\ \varepsilon_{22_{m2}}\\ \varepsilon_{12_{m3}}\end{bmatrix} = [\boldsymbol{N1}]\begin{bmatrix}\varepsilon_{11_{m1}}\\ \varepsilon_{22_{m2}}\\ \varepsilon_{12_{m3}}\end{bmatrix}$$

$$\varepsilon_n = \begin{bmatrix}\varepsilon_{13}\\ \varepsilon_{23}\\ \varepsilon_{33}\end{bmatrix} = \begin{bmatrix}N_{m1} & 0 & 0\\ 0 & N_{m2} & 0\\ 0 & 0 & 1\end{bmatrix}\begin{bmatrix}\varepsilon_{13_{m1}}\\ \varepsilon_{23_{m2}}\\ \varepsilon_{33}\end{bmatrix} = [\boldsymbol{N2}]\begin{bmatrix}\varepsilon_{13_{m1}}\\ \varepsilon_{23_{m2}}\\ \varepsilon_{33}\end{bmatrix}$$

where the matrices $\boldsymbol{N1}$ and $\boldsymbol{N2}$ are introduced. The geometrical relations are

$$\begin{aligned}\varepsilon_p &= F_\tau(\boldsymbol{D}_p + \boldsymbol{A}_p)(N_i\boldsymbol{I})\boldsymbol{q}_{\tau_i}\\ \varepsilon_n &= F_\tau(\boldsymbol{D}_{n\Omega} - \boldsymbol{A}_n)(N_i\boldsymbol{I})\boldsymbol{q}_{\tau_i} + F_{\tau_{,z}}\boldsymbol{A}_{nz}(N_i\boldsymbol{I})\boldsymbol{q}_{\tau_i}\end{aligned}$$

where $\boldsymbol{I}$ is a 3×3 identity matrix. If the MITC technique is applied to the strains, the geometrical relations will be re-written in the following manner:

$$\begin{aligned}\varepsilon^{\tau}_{p_{im}} &= F_\tau[\boldsymbol{C}_{3_{im}}]\boldsymbol{q}_{\tau_i}\\ \varepsilon^{\tau}_{n_{im}} &= F_\tau[\boldsymbol{C}_{1_{im}}]\boldsymbol{q}_{\tau_i} + F_{\tau_{,z}}[\boldsymbol{C}_{2_{im}}]\boldsymbol{q}_{\tau_i}\end{aligned}$$

where the introduced matrixes are

$$[\boldsymbol{C}_{1_{im}}] = [\boldsymbol{N2}]\begin{bmatrix}[(\boldsymbol{D}_{n\Omega} - \boldsymbol{A}_n)(N_i\boldsymbol{I})]_{m1}(1,:)\\ [(\boldsymbol{D}_{n\Omega} - \boldsymbol{A}_n)(N_i\boldsymbol{I})]_{m2}(2,:)\\ [(\boldsymbol{D}_{n\Omega} - \boldsymbol{A}_n)(N_i\boldsymbol{I})](3,:)\end{bmatrix}$$

$$[\boldsymbol{C}_{2_{im}}] = [\boldsymbol{N2}]\begin{bmatrix}[\boldsymbol{A}_{nz}(N_i\boldsymbol{I})]_{m1}(1,:)\\ [\boldsymbol{A}_{nz}(N_i\boldsymbol{I})]_{m2}(2,:)\\ [\boldsymbol{A}_{nz}(N_i\boldsymbol{I})](3,:)\end{bmatrix}$$

$$[\boldsymbol{C}_{3_{im}}] = [\boldsymbol{N1}]\begin{bmatrix}[(\boldsymbol{D}_p + \boldsymbol{A}_p)(N_i\boldsymbol{I})]_{m1}(1,:)\\ [(\boldsymbol{D}_p + \boldsymbol{A}_p)(N_i\boldsymbol{I})]_{m2}(2,:)\\ [(\boldsymbol{D}_p + \boldsymbol{A}_p)(N_i\boldsymbol{I})]_{m3}(3,:)\end{bmatrix}$$

$(1,:)$, $(2,:)$ and $(3,:)$ indicate that the first, second or third line of the relative matrix is considered, respectively.

REFERENCES

1. L. Euler. *Methodus Inveniendi Lineas Curvas Maximi Minimive Proprietate Gaudentes, Sive Solutio Problematis Isoperimetrici Lattissimo Sensu Accepti*, chapter De Curvis Elasticis. Bousquet, Lausanne and Geneva, 1744.
2. S.P. Timoshenko. On the corrections for shear of the differential equation for transverse vibrations of prismatic bars. *Philosophical Magazine*, 41:744–746, 1921.
3. S.P. Timoshenko. On the transverse vibrations of bars of uniform cross section. *Philosophical Magazine*, 43:125–131, 1922.
4. K. Kapania and S. Raciti. Recent advances in analysis of laminated beams and plates, part I: Shear effects and buckling. *AIAA J.*, 27(7):923–935, 1989. doi: 10.2514/3.10202.
5. V.V. Novozhilov. *Theory of elasticity*. Pergamon Press, Oxford, 1961.
6. W. Wagner and F. Gruttmann. A displacement method for the analysis of flexural shear stresses in thin walled isotropic composite beams. *Comput. Struct.*, 80:1843–1851, 2002.
7. R. El Fatmi. On the structural behavior and the Saint Venant solution in the exact beam theory. Application to laminated composite beams. *Comput. Struct.*, 80(16-17):1441–1456, 2002.
8. R. El Fatmi. Non-uniform warping including the effects of torsion and shear forces. Part I: A general beam theory. *Int. J. Solids Struct.*, 44(18-19):5912–5929, 2007.
9. R. El Fatmi and N. Ghazouani. Higher order composite beam theory built on Saint-Venant solution. Part-I: Theoretical developments. *Compos. Struct.*, 93(2), 2011. doi: 10.1016/j.compstruct.2010.08.024.
10. P. Ladéveze, P. Sanchez, and J. Simmonds. Beamlike (saint-venant) solutions for fully anisotropic elastic tubes of arbitrary closed cross section. *Int. J. Solids Struct.*, 41(7):1925–1944, 2004.
11. W. Yu and D.H. Hodges. Elasticity solutions versus asymptotic sectional analysis of homogeneous, isotropic, prismatic beams. *J. Appl. Mech.*, 71:15–23, 2004.
12. W. Yu and D.H. Hodges. Generalized Timoshenko theory of the variational asymptotic beam sectional analysis. *J. Am. Helicopter Soc.*, 50(1):46–55, 2005.
13. R. Schardt. Generalized beam theory-an adequate method for coupled stability problems. *Thin Wall. Struct.*, 19:161–180, 1994.
14. N. Silvestre. GBT buckling analysis of pultruded FRP lipped channel members. *Comput. Struct.*, 81(18-19):1889–1904, 2003.
15. P. Dinis, D. Camotim, and N. Silvestre. GBT formulation to analyse the buckling behaviour of thin-walled members with arbitrarily "branched" open cross-sections. *Thin Wall. Struct.*, 44(1):20–38, 2006.
16. N. Silvestre. Generalised beam theory to analyse the buckling behaviour of circular cylindrical shells and tubes. *Thin Wall. Struct.*, 45(2):185–198, 2007.
17. M. Nedelcu. Gbt formulation to analyse the behaviour of thin-walled members with variable cross-section. *Thin Wall. Struct.*, 48(8):629–638, 2010.
18. H. Hakula, Y. Leino, and J. Pitkäranta. Scale resolution, locking, and higher-order finite element modelling of shells. *Comput. Method Appl. M.*, 133:155–182, 1996.
19. C. Chinosi, L. Della Croce, and T. Scapolla. Hierarchic finite elements for thin naghdi shell model. *Int. J. Solids Struct.*, 35:1863–1880, 1998.
20. O.C. Zienkiewicz, R.L. Taylor, and J.M. Too. Reduced integration techniques in general analysis of plates and shells. *Int. J. Numer. Meth. Eng.*, 3:275–290, 1971.
21. H. Stolarski and T. Belytschko. *New Concepts in Finite Element Analysis*, chapter Reduced integration for shallow-shell facet elements. ASME, New York, 1981.
22. J.J. Rhiu and S.W. Lee. A new effcient mixed formulation for thin shell finite element models. *Int. J. Numer. Meth. Eng.*, 24:581–604, 1987.
23. E. Carrera. Theories and finite elements for multilayered plates and shells: a unified compact formulation with numerical assessment and benchmarking. *Arch. Comput. Method E.*, 10(3):216–296, 2003.
24. E. Carrera. Multilayered shell theories that account for a layer-wise mixed description. Part II. Numerical evaluations. *AIAA J.*, 37:1117–1124, 1999.
25. D. Chapelle and K.J. Bathe. *The finite element analysis of shells. Fundamentals.* Springer, Berlin, 2003.
26. C. Chinosi and L. Della Croce. Mixed-interpolated elements for thin shell. *Commun. Numer. Meth. En.*, 14:1155–1170, 1998.
27. M. Cinefra, C. Chinosi, and L. Della Croce. Mitc9 shell elements based on refined theories for the analysis of isotropic cylindrical structures. *Mech. Adv. Matl. Struct.*, In Press, 2011.
28. E. Carrera, G. Giunta, and M. Petrolo. *Beam Structures: Classical and Advanced Theories*. John Wiley & Sons, 2011.
29. E. Carrera and G. Giunta. Refined beam theories based on Carrera's unified formulation. *Int. J. Appl. Mech.*, 2(1):117–143, 2010.
30. E. Carrera, G. Giunta, P. Nali, and M. Petrolo. Refined beam elements with arbitrary cross-section geometries. *Comput. Struct.*, 88(5–6):283–293, 2010. DOI: 10.1016/j.compstruc.2009.11.002.

31. E. Carrera, G. Giunta, and M. Petrolo. *A Modern and Compact Way to Formulate Classical and Advanced Beam Theories*, chapter 4, pages 75–112. Saxe-Coburg Publications, Stirlingshire, UK, 2010. doi: 10.4203/csets.25.4.
32. E. Carrera, M. Petrolo, and E. Zappino. Performance of cuf approach to analyze the structural behavior of slender bodies. *J. Struct. Eng.*, 2012. In Press, doi:10.1061/(ASCE)ST.1943-541X.0000402.
33. E. Carrera, M. Petrolo, and P. Nali. Unified formulation applied to free vibrations finite element analysis of beams with arbitrary section. *Shock Vib.*, 18(3):485–502, 2011. doi: 10.3233/SAV-2010-0528.
34. E. Carrera, M. Petrolo, and A. Varello. Advanced beam formulations for free vibration analysis of conventional and joined wings. *J. Aerospace Eng.*, 2012. In Press, doi:10.1061/(ASCE)AS.1943-5525.0000130.
35. M. Petrolo, E. Zappino, and E. Carrera. Unified higher-order formulation for the free vibration analysis of one-dimensional structures with compact and bridge-like cross-sections. *Thin Wall. Struct.*, 2012. In Press.
36. S.M. Ibrahim, E. Carrera, M. Petrolo, and E. Zappino. Buckling of composite thin walled beams by refined theory. *Compos. Struct.*, 94(2):563–570, 2012.
37. E. Carrera and M. Petrolo. Refined beam elements with only displacement variables and plate/shell capabilities. *Meccanica*, 47(3), 2012. doi: 10.1007/s11012-011-9466-5.
38. E. Carrera and M. Petrolo. Refined one-dimensional formulations for laminated structure analysis. *AIAA J.*, 50(1), 2012. doi: 10.2514/1.J051219.
39. E. Carrera and M. Petrolo. Guidelines and recommendations to construct theories for metallic and composite plates. *AIAA J.*, 48(12):2852–2866, 2010. doi: 10.2514/1.J050316.
40. E. Carrera and M. Petrolo. On the effectiveness of higher-order terms in refined beam theories. *J. App. Mech.*, 78(3), 2011. doi: 10.1115/1.4002207.
41. E. Carrera, F. Miglioretti, and M. Petrolo. Guidelines and recommendations on the use of higher order finite elements for bending analysis of plates. *Int. J. Comput. Meth. Eng. Sc. and Mech.*, 12(6):303–324, 2011. DOI:10.1080/15502287.2011.615792.
42. E. Carrera, F. Miglioretti, and M. Petrolo. Accuracy of refined finite elements for laminated plate analysis. *Compos. Struct.*, 93(5):1311–1327, 2011. DOI:10.1016/j.compstruct.2010.11.007.
43. E. Oñate. *Structural Analysis with the Finite Element Method: Linear Statics, Volume 1*. Springer, Barcelona, Spain, 2009.
44. P.M. Naghdi. The theory of shells and plates. *Handbuch der Phisik*, 6, 1972.
45. W.T. Koiter. On the foundations of the linear theory of thin elastic shell. In *Proc. Kon. Nederl. Akad. Wetensch.*, 1970.
46. K.J. Bathe. *Finite element procedure*. Prentice hall, Upper Saddle River, New Jersey, 1996.
47. J.N. Reddy. *Mechanics of laminated composite plates and shells. Theory and Analysis*. CRC Press, 2^{nd} edition, 2004.
48. W. Flügge. *Stresses in shells*. Springer, Berlin, 2nd edition, 1960.
49. Scordelis A.C. and K.S. Lo. Computer analysis of cylindrical shells. *J. Am. Concr. Inst.*, 61:539–560, 1964.